Influence of Convective Drying Parameters on Electrode Performance and Physical Electrode Properties

ECS Transactions, 64 (22) 57-68 (2015)
10.1149/06422.0057ecst ©The Electrochemical Society

Influence of Convective Drying Parameters on Electrode Performance and Physical Electrode Properties

B. G. Westphal[a,b,c], H. Bockholt[a,b], T. Günther[a], W. Haselrieder[a,b,c], A. Kwade[a,b,c]

[a] Institute for Particle Technology, Technische Universität Braunschweig, Volkmaroder Straße 5, 38104 Braunschweig, Germany
[b] Battery LabFactory Braunschweig (BLB), Technische Universität Braunschweig, Langer Kamp 19, 38106 Braunschweig, Germany
[c] Lion Engineering GmbH, Rebenring 33, 38106 Braunschweig, Germany

In the present work two of the various drying process parameters, air temperature and nozzle speed, are studied and their influence on the electrode's physical properties is examined by different mechanical and electrical analyzes. It was found that elasticity, electrical volume resistivity and adhesion strength of the coating to the substrate, can be dependent on process parameters used for manufacturing. These properties are also influenced by the electrode's mass loading and its recipe, as the total solvent content and therefore the drying time plays an important role. Assuming binder demixing during drying allows explaining the results, since evaporating solvent induces a temperature dependent compensational flow of solvent and solved binder. If immobilization occurs faster than compensational flow can cause significant demixing, no binder gradient emerges. The driving force counteracts the drying time, but increases demixing, so that optimum drying conditions exist for each mass loading and solid content.

Introduction

As the need for nonpolluting individual mobility is rising, the production processes of lithium-ion batteries are gaining much more attention (1). Although a lot of research for new battery materials (2-6) or even for alternative battery technologies (7-9) is done, the state of the art production process for large scale automotive lithium-ion batteries is still not completely explored. To get as close as possible to the theoretical performance of the used materials, an optimized process which includes a deep understanding of its influences on electrode structure and in the end on cell performance, is essential (10-12). For this reason the drying process, as one of the key-process-steps in the electrode production process, is examined in this publication.

The drying of the electrodes takes place subsequent to the coating and is therefore depending on the coating speed, which is itself restricted by the used coating device and the suspension properties (13). As enhanced production speed is directly correlated to higher electrode output and thus higher economic benefit, companies try to increase the production speed. This results in an increased dryer length L, hence the same amount of

solvent as on slower production speeds, needs to be evaporated and the drying conditions cannot be intensified arbitrarily.

Besides the economic reason, drying is important, because it fixes the coating structure by evaporation of the solvent, and thus influences the sedimentation of active material particles and the formation of the binder and carbon black matrix in a crucial way. As the binder and carbon black matrix is important for electric conductivity and electrolyte penetration (14, 15) its optimization and the avoidance of reported demixing processes (16, 17) is an urgent requirement when producing electrodes. Dependent on the drying parameters the intensity and therefore the driving force for binder demixing, cracking and building of electrode network can be changed significantly. Temperature and air speed as drying parameters are discussed in this study and their influence on artificial graphite anodes with different mass loadings are examined.

Experimental

Materials and Composition

For all experiments the materials and compositions given in table I were used. The solid content for anodes was adjusted to 58 wt% while dispersing and diluted before coating to 45 wt%. The suspensions were produced using N-Methyl-2-Pyrrolidone (NMP) as solvent, polyvinylidene difluoride (PVDF) as binder and electrodes were coated on 10 µm-copper-foil.

TABLE I. Materials and Recipe for Anodes

Type of Component	Amount in Mixture
Artificial Graphite	91 wt%
PVDF Binder	3 wt%
Carbon Black	6 wt%
NMP	35 %

Dry and Wet Mixing Process

Dry and wet mixing was carried out in a planetary mixer (PMH 10, Netzsch-Feinmahltechnik, Selb, Germany), which has a fast rotating toothed disk and a slow rotating cross-blade agitator, as well as a wall scraper. These three installations rotate additionally around a common central axes (typical planetary mixing system). The mixing parameters were kept constant and the reproducibility was found to be excellent. The chosen parameter-set for the production of 6 liters of suspension is summarized in table II.

TABLE II. Parameter-Set for Suspension Production in Planetary Mixer

Parameter	Dry Mixing	Wet Mixing
Butterfly Stirrer Speed [rpm]	1000	2500
Flow Blade Stirrer Speed [rpm]	60	200
Mixing Time [min]	5	60

Coating and Drying Process

A pilot-plant continuous convective coater/dryer combination (LabCo, Kroenert GmbH & Co. KG, Hamburg, Germany) with three individual adjustable drying segments and a total dryer length of six meters in combination with a comma bar (used for film generation) plus reverse roll (used for film transfer) coating unit is used to dry the wet film on the substrate. For each examined process variation (see results section) the same suspension was used and the experiment was carried out at the same day in order to avoid influences from humidity and room temperature changes.

TABLE III. Parameter-Set for Continuous Coating and Drying Device

Parameter	Coating	Drying
Web Speed [m/min]	2	2
Coating Method	Comma Bar + Reverse Roll	-
Coating Gap [µm]	75 - 240	-
Drying Temperature [°C]	-	80 - 130
Calculated Nozzle Speed [m/s]	-	4 - 25
Airflow / Nozzle Setup	-	Diffused / Direct

Analyses

Adhesion Strength Measurement: The measurement setup is placed into a materials testing machine (Z020, Zwick GmbH & Co. KG, Ulm, Germany), in order to apply a defined pressure on an electrode sample placed between two plane parallel plates, each covered with double-sided adhesive tape with high adhesive power. After the dwell time has passed the two plates are quickly moving in opposite directions to achieve a pull-off of the coating from the substrate. The maximum force F needed to pull-off the coating from the current collector is detected with 2 kHz and the adhesion strength σ can be calculated, taking the sample area A into account. Further testing parameters can be found in table IV and additional information in (18).

TABLE IV. Parameter-Set for Adhesion Strength Measurement

Parameter	Value
Feed Control	Force Controlled
Data Acquisition Rate [Hz]	2000
Compression Stress [kPa]	600
Compression Velocity [mm/min]	0.75
Dwell Time [s]	30
Pull-Off Velocity [mm/min]	100

Resistivity Measurement: A Current Transit Method (CTM) is used to determine the electric volume resistivity of the electrode. The current is provided using a RESISTOMAT® 2329 (Burster Präzisionsmesstechnik GmbH & Co KG, Gernsbach, Germany) and is applied to the sample by two contact plates that are connected to a materials testing machine (Z020, Zwick GmbH & Co. KG, Ulm, Germany), in order to apply a defined contact stress during measurement. Table V shows the setup used for the resistivity measurements, further information can be found in (19).

TABLE V. Parameter-Set for Resistivity Measurement

Parameter	Value
Feed Control	Force Controlled
Contact Area [cm²]	1.13
Contact Stress [kPa]	350
Compression Velocity [mm/min]	0.75
Dwell Time [s]	5
Applied Current [mA]	10

Micro-Compression: The nanomechanical testing machine UNAT (ASMEC GmbH, Radeberg, Germany) is used to determine the elastic and plastic deformation energy of the electrodes. A flat punch with a diameter of 100 µm is used to compress the electrode up to 10 % of coating thickness and the resulting force displacement data is measured. The force displacement graphs can be used to calculate the elastic and plastic as well as the total deformation work.

TABLE VI. Parameter-Set for Micro-Compression -

Parameter	Value
Feed Control	Distance Controlled
Indenter Tip	Flat Punch
Indenter Diameter [µm]	100
Compression Velocity [mN/s]	2,8
Indentation Depth [% Coating Thickness]	10
Minimum Number of Valid Indents	50

Results and Discussion

Reasons for Demixing Phenomena

In order to provide easier access to the subsequent displayed results a short explanation of the assumed mechanism is given at the beginning of this section.

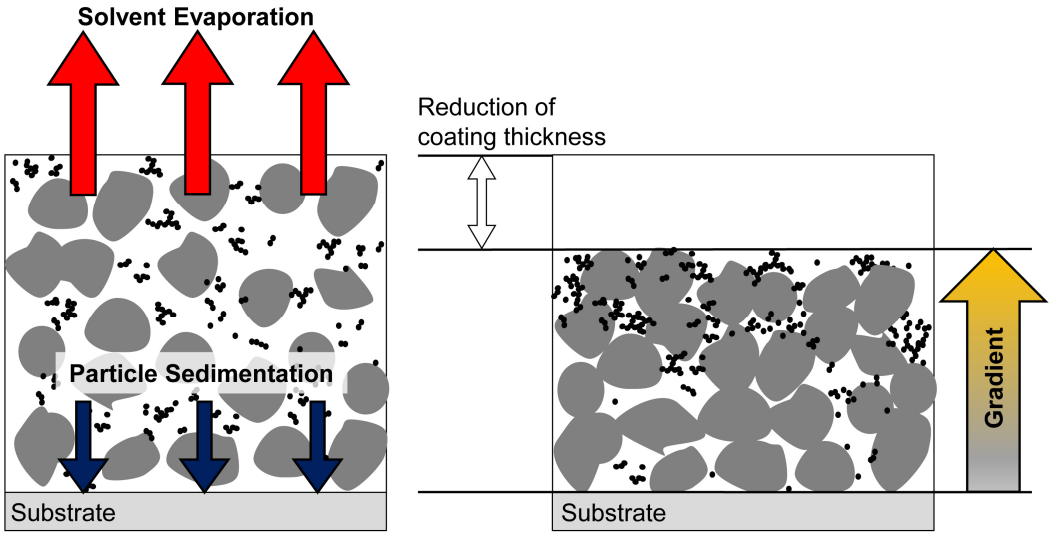

Figure 1. Schematic drawing of the two most important driving forces for demixing processes in electrodes for lithium-ion batteries during drying

Figure 1 shows schematically the potential driving forces for demixing processes in a multicomponent electrode suspension. The black dots do not necessarily represent the carbon black, used to create sufficient electronic conductivity inside the electrode, as it might also be the isolating binder, which is responsible for mechanical stability of the electrode's coating. One of the potential driving forces, while the coating is still wet, is particle sedimentation, due to an instable suspension, low solid contents or active materials with a high solid density. The other driving force, solvent evaporation, can be considered much more dominant, as suspensions for lithium-ion batteries feature most often high solid contents and sort of stable suspensions. During drying in a unidirectional system the solvent has to evaporate at the coatings surface, creating a driving force towards the coating/air interface, being responsible for a potential demixing of dissolved and/or lightweight components. At the same time, the solvent can be pushed to the top of the wet coating, as the dense active material particles sediment down to the substrate.

Influence of Drying Temperature

One of the most evident parameters of the drying process is the surface T. In order to allow a better interpretation of the acquired data the temperature is not varied along the three drying segments. In this section the airflow of all the drying nozzles shown in figure 4 is kept constant at 17 m/s for upper and 34 m/s for lower nozzle. Other coating parameters can be found in table III.

In this chapter relatively thick graphitic coatings, with a mass loading ML of 10.5 mg/cm², are characterized by the methods described in the experimental section. Figure 2 shows a decreasing adhesion strength σ with an increasing drying temperature, as well as a decrease in electrode resistance R.

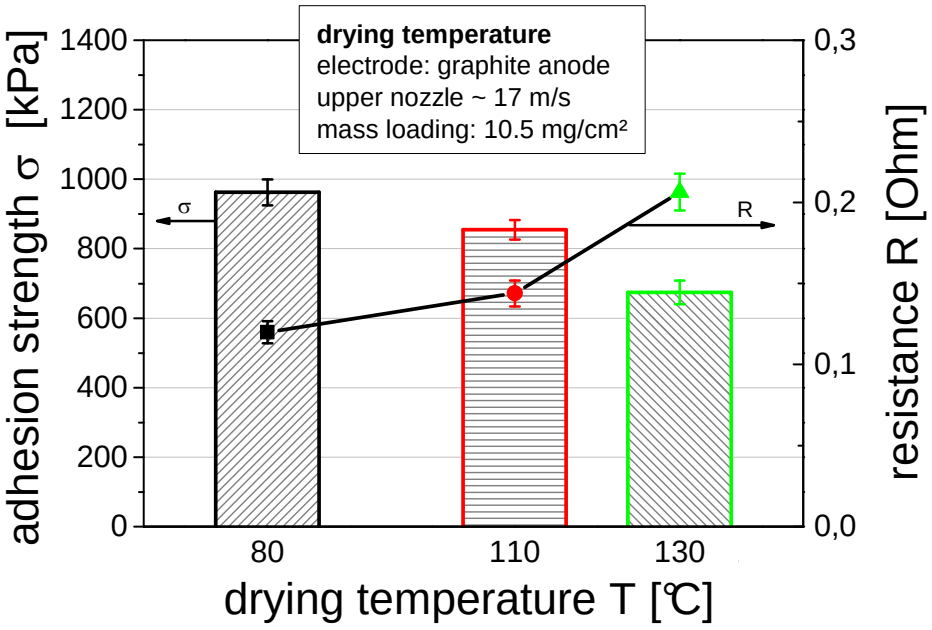

Figure 2. Decreasing adhesion strength and increasing resistance with increasing drying temperature and thus higher demixing driving force

These changes can be explained by a demixing of the binder during drying. A higher driving force for binder demixing originates from increasing drying temperatures, as the

wet coating is heated up faster and the solvent evaporation is accelerated. The evaporating solvent induces a temperature dependent compensational flow of NMP and the solved binder. As the binder cannot cross the solvent/air interface, it concentrates at the electrodes surface. The explained binder demixing causes a lack of binder at the substrate/coating interface leading to a decrease in connecting binder bonds and finally to a reduced coating adhesion (shown in figure 2). Furthermore the accumulation of isolating binder at the electrode's surface is the reason for the resistance increase with higher temperature, as increasing temperature leads to an increased demixing. As a consequence the suggested binder demixing can be proofed indirectly by measuring the physical properties of the manufactured electrode.

This demixing takes place until the structure of the electrode is fixed, as further drying leads to a subsiding fluid level (18). It is believed that there is no significant reorganization or movement of the particles when the electrode's surface is dry. This is indicated by the surface temperature T_s reaching the ambient drying temperature, thus the change between constant rate period and falling rate period (see figure 4).

Further approval can be achieved by micro-compression measurements. Figure 3 shows the cumulative distribution of the ratio of elastic ($W_{elastic}$) to total (W_{total}) indentation work for different drying temperatures. An increase of the median $(W_{elastic}/W_{total})_{50}$ with rising temperature can be observed. This is a result of the increase in binder demixing as the binder and the carbon black network are responsible for the elasticity in an electrode. Therefore higher binder concentration at the electrode's surface results in an increase in elastic behavior.

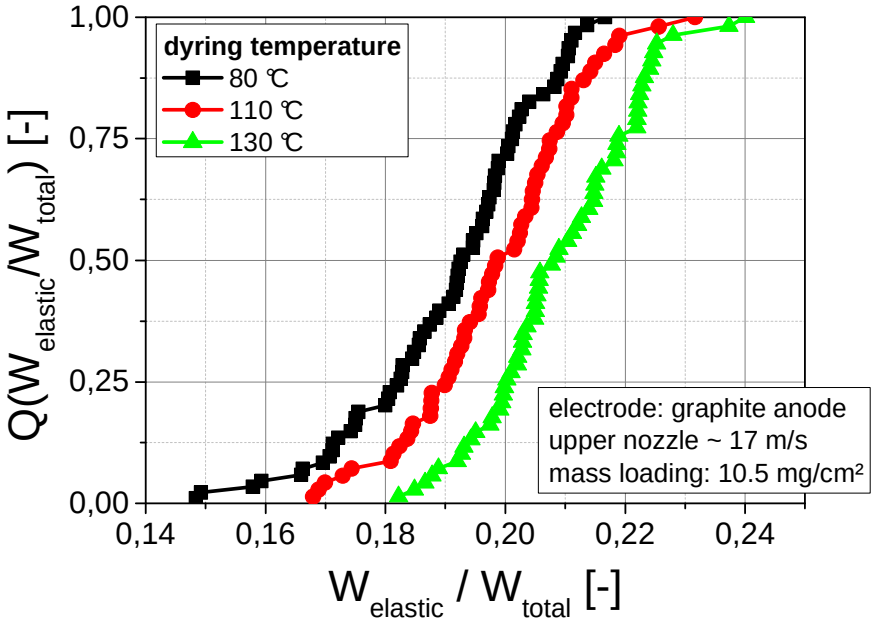

Figure 3. Cumulative distribution of micro-compression results, showing the temperature dependent change of elasticity

Influence of coating mass loading

As temperature and total amount of solvent determine the drying speed and thus the point at which the electrode's structure is immobilized, this chapter will examine the

influence of coating thickness or mass loading, respectively. Figure 4 shows the measured surface temperature of the coated substrate (solid line) and the uncoated substrate (dashed line) along the length of the dryer L. As already mentioned above, it is assumed, that there is no change in electrode structure after the electrode's surface is dry. As the point where the surface temperature of the coated substrate reaches the temperature of the uncoated substrate (thus the surrounding temperature) marks the moment where the surface is dry, thus there will be no important structural changes beyond this.

Figure 4 shows, for the given mass loading, that the dryer length, which is needed to achieve a fixed electrode structure, increases with decreasing temperature. The temperature rise at the beginning and the drop at the end of the dryer are caused by the dryer's in- and outlet, at which air with room temperature from outside the dryer is sucked in. As a result, an elongation of the constant rate period and therefore an elongated time for immobilization of the particles can be observed, if either temperature is decreased or mass loading is increased.

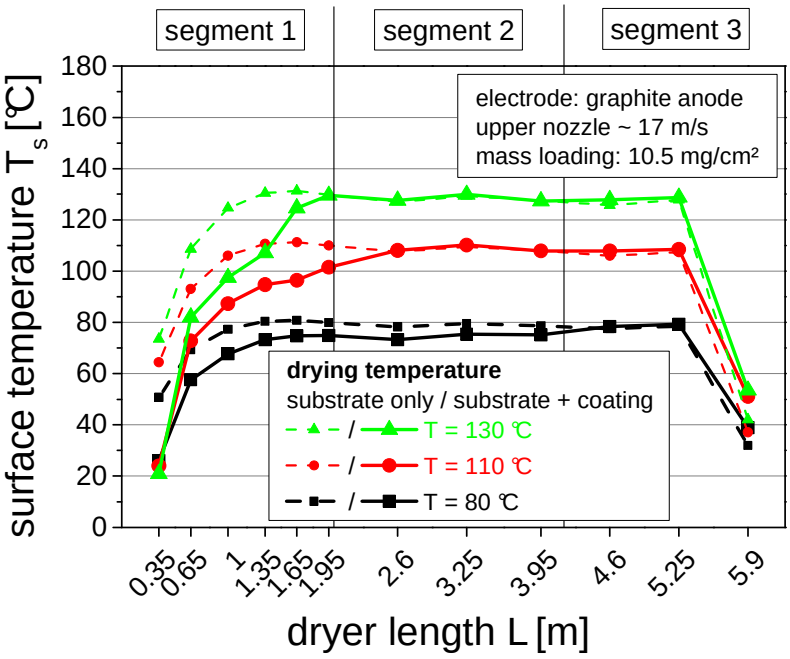

Figure 4. Surface temperatures of graphite anodes and substrate along the dryer length at different drying temperatures

If immobilization of the particles inside of the electrode structure is faster than the compensational flow of the solvent to the electrodes surface, demixing of binder is drastically reduced. The lower the amount of total solvent inside the wet coating and the higher the temperature, the faster the total solvent volume will be evaporated. Figure 5 shows that the electrical resistance of low mass loadings (3.5 and 5.4 mg/cm²) is almost not influenced by rising temperature, as the total amount of solvent is low and structure immobilization is too fast to cause a significant demixing of the binder. As there is only a small resistance increase measurable, almost no isolating binder deposition for low mass loadings at the electrode's surface is expected. It should be mentioned, that fast drying can lead to coating defects, like cracks or trapped vapor bubbles, however drying was carried out in a way, that none of them were observed during this study.

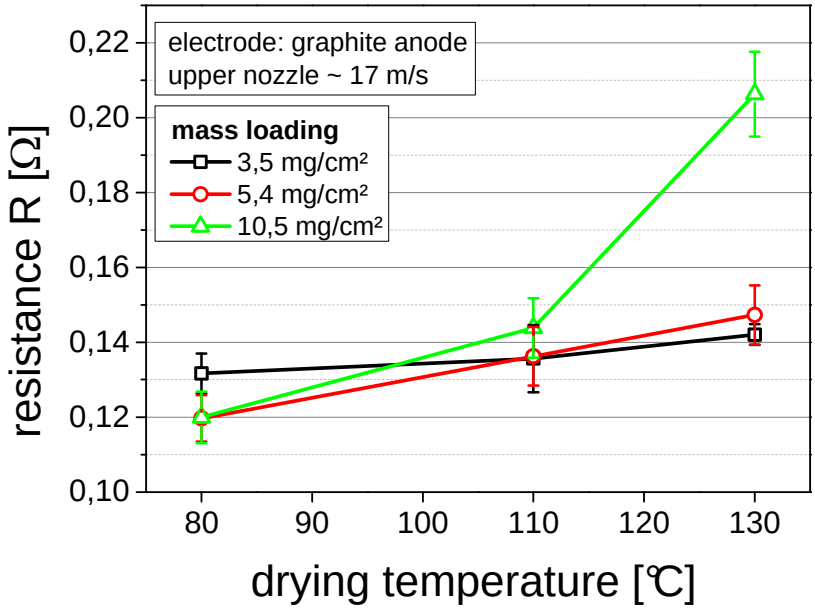

Figure 5. Influence of drying temperature and mass loading on electrode resistance

Thick electrodes with high mass loadings show a different behavior. As the constant rate period is long enough for demixing to take place, an increase in temperature results in a higher driving force for binder demixing and finally in an increasing resistance.

The importance of total solvent mass and driving force gets more obvious, when normalized adhesion strength σ_n is monitored as a function of temperature and mass loading. Figure 6 shows that the normalized adhesion strength is almost independent of mass loading if the drying temperature is quite low with 80 °C.

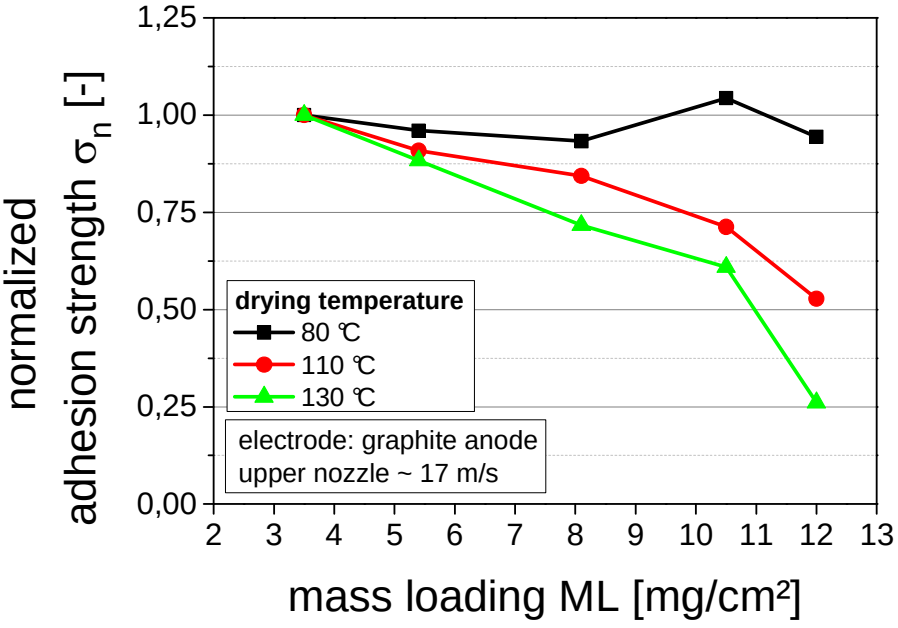

Figure 6. Adhesion strength normalized to adhesion strength at 3,5 mg/cm², showing higher decrease at higher temperatures

As soon as temperature increases to 110 °C the driving force is strong enough and if mass loading is sufficient high (at least 5.4 mg/cm² or higher) the drying time is long enough for binder demixing to occur. With further increase in mass loading normalized adhesion strength decreases to 52 % at 12 mg/cm² compared to a mass loading of 3.5 mg/cm². If temperature is increased to 130 °C the demixing effect gets stronger with increasing mass loading and therefore adhesion strength declines to 25 % at 12 mg/cm² compared to a mass loading of 3.5 mg/cm².

These results clearly show that not only the strength of the drying force is responsible for binder demixing, it is a combination of driving force and time in which the demixing can take place before the final electrode structure is set. The driving force counteracts the drying time but enhances demixing mechanism, so that optimum drying conditions exist for each mass loading and each suspension recipe.

Influence of Nozzle Speed / Air Flow

Figure 7 shows a picture of the drying nozzles, the infrared-sensor and the web, as well as the direct (striped arrows) and diffuse (checkered arrows) nozzle air streams. The upper nozzles provide the opportunity to change air stream conditions. If the diffuse slots at the sides of the nozzles are opened, the direct nozzle slots are closed and vice versa. In contrast to direct drying conditions, the nozzle speed at diffuse drying conditions is lower and not directed to the coatings surface. All given nozzle speeds are calculated from air volume depending on fan speed, and represent the speed immediately after leaving the nozzle. In contrast to the section “Influence of Drying Temperature” the temperature is kept constant at 110 °C throughout all experiments in this chapter.

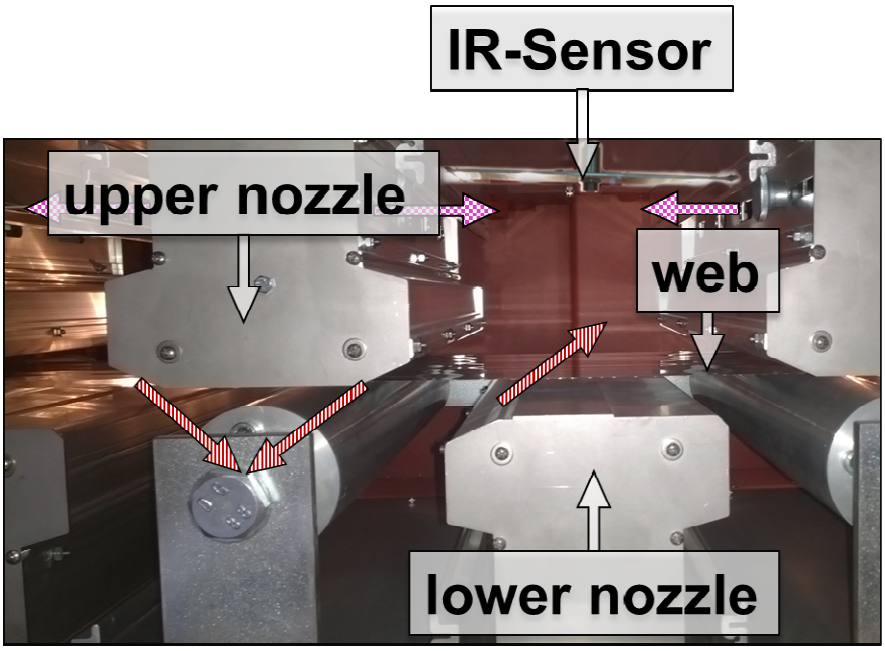

Figure 2. Arrangement of drying nozzles, web and IR-Sensors. Striped arrows represent direct air flow and checkered arrows represent diffuse air flow

Direct drying can be considered as a much higher demixing driving force compared to diffuse drying, so it is more likely to change electrode properties. This property change is

proven by the results in figure 8, showing a drop in adhesion strength if mass loading and therefore drying time is high enough. The reason for this drop was already stated above, as the polymer binder is driven to the electrode's surface, creating a lack of binder at the substrate/coating interface, and therefore a decreased adhesion strength.

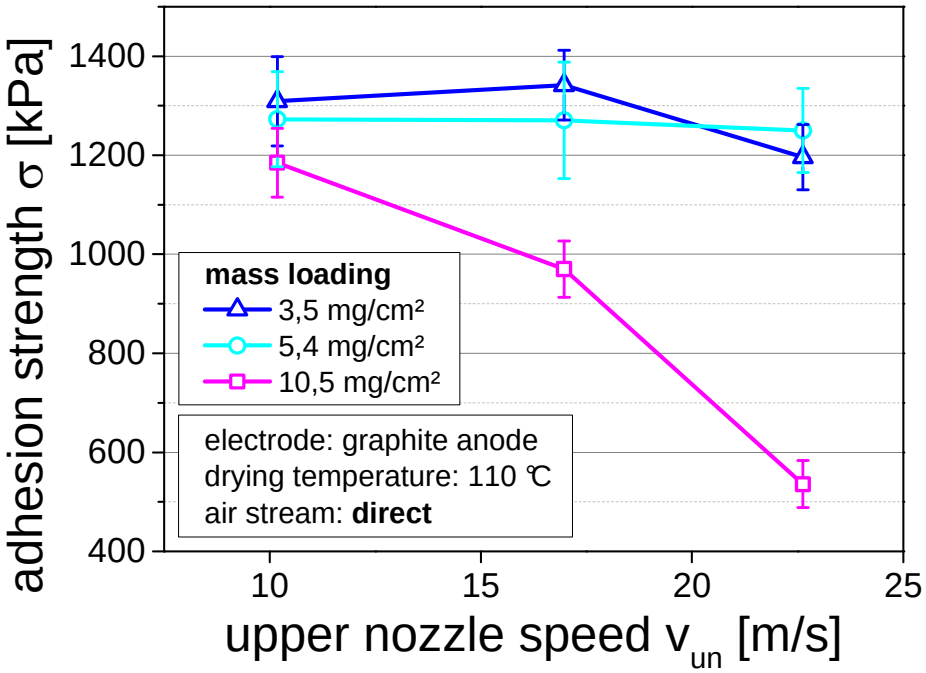

Figure 8. Adhesion strength depending on mass loading and upper nozzle speed

Increasing drying intensity evoked by higher upper nozzle speeds v_{un} leads to a decrease in adhesion strength if mass loading and thus drying time is high enough for binder demixing to occur. In contrast to that, lower mass loadings are almost not influenced by the upper nozzle speed, as the drying is too fast to create a binder gradient by demixing.

Even at diffuse, and thus less intense, drying conditions a higher driving force induces demixing, as the results from resistance measurements in figure 9 (left) illustrate.

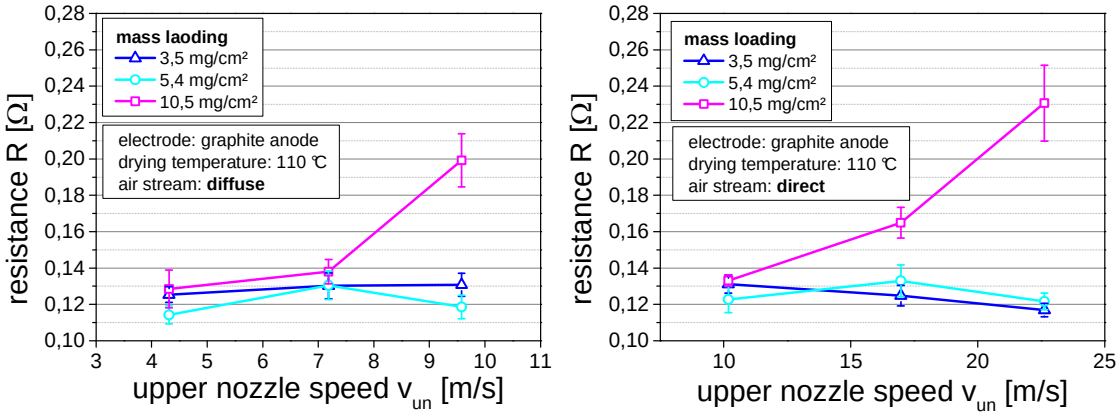

Figure 9. Increase of resistance at high mass loadings and high nozzle speeds for diffuse (left) and direct (right) air stream at 110 °C

The demixing, occurring after diffuse drying, is only observed at the highest upper nozzle speed in combination with the highest mass loading and is less distinct compared to the results for direct drying conditions (figure 9, right). In both cases (direct and diffuse drying) low mass loadings are not affected by increasing driving force, as the drying process is too fast and the electrode's structure is immobilized before binder demixing sets in.

Conclusions

The presented results elucidate that elasticity, electrical volume resistivity and adhesion strength between coating and substrate, are highly dependent on process parameters used for electrode manufacturing. This can be explained by binder demixing during drying, as a lack of binder at the substrate/coating interface leads to a decrease in connecting binder bonds and finally to a reduced coating adhesion. Furthermore the accumulation of isolating and elastic binder at the electrode's surface is the reason for a resistance and elasticity increase. As a consequence the suggested binder demixing can be proofed indirectly by measuring the physical properties of the manufactured electrode.

Although temperature, nozzle speed and air flow conditions have been used to change drying intensity a more generalized statement can be given, as it was clearly shown, that not only the strength of the drying force is responsible for binder demixing. Binder gradient formation is rather a combination of driving force intensity and time in which the demixing can take place before the final electrode structure is fixed. The driving force counteracts the drying time but enhances demixing mechanism, so that optimum drying conditions exist for each mass loading and each suspension recipe, as they influence the time span until immobilization of particles.

Acknowledgments

The authors gratefully thank the German Federal Ministry for Education and Research (BMBF) for the financial support and Project Management Karlsruhe (PTKA-PFT) branch office Dresden for financial management of the project "Integriertes Fertigungskonzept für advanced automotive Batteries (iFaaB)".

References

1. J. Li, C. Daniel and D. Wood, *Journal of Power Sources*, **196**, 2452 (2011).
2. C. M. Hayner, X. Zhao and H. H. Kung, *Annual Review of Chemical and Biomolecular Engineering*, **3**, 445 (2012).
3. J. W. Fergus, *Journal of Power Sources*, **195**, 939 (2010).
4. L. Ji, Z. Lin, M. Alcoutlabi and X. Zhang, *Energy and Environmental Science*, **4**, 2682 (2011).
5. G. Mulder, N. Omar, S. Pauwels, M. Meeus, F. Leemans, B. Verbrugge, W. De Nijs, P. Van den Bossche, D. Six and J. Van Mierlo, *Electrochimica Acta*, **87**, 473 (2013).
6. J. Xiao, J. Zheng, X. Li, Y. Shao and J. G. Zhang, *Nanotechnology*, **24**, 424004 (2013).
7. V. Etacheri, R. Marom, R. Elazari, G. Salitra and D. Aurbach, *Energy & Environmental Science*, **4**, 3243 (2011).

8. M. M. Thackeray, C. Wolverton and E. D. Isaacs, *Energy & Environmental Science*, **5**, 7854 (2012).
9. T. N. P. C. (NPC), Advanced Batteries: "Beyond Li-ion", in *Topic Paper*, The National Petroleum Council (NPC) (2012).
10. H. Bockholt, W. Haselrieder and A. Kwade, *ECS Transactions*, **50**, 25 (2013).
11. W. Haselrieder, S. Ivanov, H. Y. Tran, S. Theil, L. Froböse, B. Westphal, M. Wohlfahrt-Mehrens and A. Kwade, *Progress in Solid State Chemistry* (2014).
12. H. Y. Tran, G. Greco, C. Täubert, M. Wohlfahrt-Mehrens, W. Haselrieder and A. Kwade, *Journal of Power Sources*, **210**, 276 (2012).
13. J. Kaiser, V. Wenzel, H. Nirschl, B. Bitsch, N. Willenbacher, M. Baunach, M. Schmitt, S. Jaiser, P. Scharfer and W. Schabel, *Chemie Ingenieur Technik*, **86**, 695 (2014).
14. R. Dominko, M. Gaberscek, J. Drofenik, M. Bele, S. Pejovnik and J. Jamnik, *Journal of Power Sources*, **119-121**, 770 (2003).
15. G. Liu, H. Zheng, A. S. Simens, A. M. Minor, X. Song and V. S. Battaglia, *Journal of the Electrochemical Society*, **154**, A1129 (2007).
16. H. Hagiwara, W. J. Suszynski and L. F. Francis, *Journal of Coatings Technology and Research* (2013).
17. C. C. Li and Y. W. Wang, *Journal of the Electrochemical Society*, **158**, A1361 (2011).
18. E. C. Childs and M. Bybordi, *Water Resources Research*, **5**, 446 (1969).